Applied Surface Science 666 (2024) 160340

Contents lists available at ScienceDirect

Applied Surface Science

journal homepage: www.elsevier.com/locate/apsusc

Full length article

A Blyholder mechanism in the chemisorption of N_2O on Ni(111) – studied with Auger-photoelectron coincidence spectroscopy

Fredrik O.L. Johansson [a,b,*], Lucas M. Cornetta [a,c], Elin Berggren [a], Artem Kuklin [a], Yi-Chen Weng [a], Swarnshikha Sinha [d,e], Danilo Kühn [d], Alexander Föhlisch [d,e], Hans Ågren [a], Andreas Lindblad [a]

[a] Division of X-ray Photon Science, Department of Physics and Astronomy, Uppsala University, Box 516, Uppsala, 751 20, Sweden
[b] Sorbonne Université, CNRS, Institut des NanoSciences de Paris, INSP, 4 pl. Jussieu, Paris, F-75005, France
[c] Instituto de Física da Universidade de São Paulo, Universidade de São Paulo, São Paulo, Brazil
[d] Institute Methods and Instrumentation for Synchrotron Radiation Research PS-ISRR, Helmholtz-Zentrum Berlin für Materialien und Energie, Albert-Einstein-Straße 15, Berlin, 12489, Germany
[e] Institut für Physik und Astronomie, Universität Potsdam, Karl-Liebknecht-Strasse 24-25, Potsdam, 14476, Germany

ARTICLE INFO

Keywords:
Auger-photoelectron coincidence spectroscopy
Blyholder model
Heterogeneous catalysis

ABSTRACT

In heterogeneous catalysis the surface-adsorbate bond strength is critical for the function of the system. Here we study a series consisting of multilayer, bilayer and monolayer N_2O on Ni(111) and employ Auger-photoelectron coincidence spectroscopy (APECS) to study the interaction between the molecule and the substrate directly. We observe intensity in the nitrogen Auger spectra that arise from the interaction between molecule and surface (not observed in free molecules) whereas the oxygen spectra are thickness-independent. Since the two nitrogen atoms of N_2O are chemically inequivalent we can assign the intensity present in the bilayer and monolayer cases to orbitals centered on the terminal nitrogen which is closest to the Ni(111) surface. Using *ab initio*, molecular dynamics and solid-state density functional theory calculations we infer a Blyholder model of the surface bond as consisting of donation from the terminal nitrogen lone-pair valence orbital with back-donation from the metal into the unoccupied orbitals on that nitrogen. This coincidence technique can readily be used to study substrate–adsorbate interactions directly with chemical and orbital specificity — this opens up prospects to study fundamental steps of molecular adsorption and heterogeneous catalysis with unprecedented detail.

1. Introduction

The interaction between metal surfaces and molecules constitutes a challenging and important area of study not the least for applications in catalysis. The oxides of nitrogen (NO_x) play a particularly important role as they are products from combustion and thus contribute to the anthropogenic concentration in the atmosphere of these gases. The main source of NO_x is from surface emissions of nitrous oxide, N_2O, which also is the third most significant greenhouse gas [1]. N_2O as an ozone-depleting agent is predicted to remain the main driver of ozone depletion during the 21st century [2].

N_2O is a triatomic molecule with the configuration N···N···O that is linear in the isolated case with the terminal (N_T) and central (N_C) nitrogen atoms being chemically inequivalent. The N_T–N_C bond is 1.126 Å and the N_C–O bond is 1.191 Å. [3] N_2O is an obvious candidate for heterogeneous catalysis since it is thermodynamically unstable with respect to N_2 and O_2 (standard enthalpy of formation $\Delta_f H^\circ$ at 82 kJ/mol) but with a high activation energy barrier [4].

Catalytic conversion of N_2O into non-pollutant components is an active challenge for the surface science community [5,6] and the development of catalytic converters in combustion engines (reviewed by [7]) is a success story for the field. If new fuels (e.g. NH_3 as an alternative to H_2 [8]) or energy conversion systems like fuel cells [9] are to be employed the problem of removing pollutants remain.

Nitrous oxide has been extensively studied in its own regard using electron spectroscopy. Since the N_T and $N_C$have different chemical surrounding, both core level and unoccupied orbitals can be studied, with electrons [10] and tunable X-rays (e.g. from synchrotrons) to obtain information about site specific excitations into different orbitals in the electronic structure [11–13].

An interesting application for this is that N_2O decomposition on Ni surfaces can be used to measure Ni particle sizes in catalyst via pulse titration of the gas over the catalyst [14].

* Corresponding author at: Division of X-ray Photon Science, Department of Physics and Astronomy, Uppsala University, Box 516, Uppsala, 751 20, Sweden.
E-mail address: fredrik.johansson@physics.uu.se (F.O.L. Johansson).

https://doi.org/10.1016/j.apsusc.2024.160340
Received 7 March 2024; Received in revised form 17 May 2024; Accepted 19 May 2024
Available online 21 May 2024
0169-4332/© 2024 The Author(s). Published by Elsevier B.V. This is an open access article under the CC BY license (http://creativecommons.org/licenses/by/4.0/).

The adsorption of N_2O on various metal surfaces has been extensively studied as reviewed by Zeigarnik [15]. From early studies on Ni [16] to molecular orientation after physisorption on Ni(111) surface [3], and further: monolayers on Ag [17] and *ab initio* modeling of the self-assembly on these surfaces [18]. Similar to NO_2 and N_2, the decomposition of N_2O has also been studied on various surfaces including Ni(110) [19]. Kodama et al. have also shown that N_2O does not decompose on fcc(111) faces, but on the vicinal (755) surface of Ni(111) it occurs while step-sites are available and when those are saturated by O, one of the decomposition products, further adsorption leave the N_2O intact [20].

The chemisorption bond of molecules on metal surfaces may in some instances be conceptualized by the Blyholder model, where donation of HOMO (highest occupied molecular orbital) electron density from the molecule to the surface is compensated by a back-donation of electron density from the surface into the LUMO (lowest unoccupied molecular orbital) to keep the system charge neutral. A classical example is CO chemisorption on Pt(111) where the 2π and 5σ orbitals are involved in the back-donation and donation [21].

The electronic ground state of N_2O is

$$1\sigma^2 2\sigma^2 3\sigma^2 4\sigma^2 5\sigma^2 6\sigma^2 1\pi^4 7\sigma^2 2\pi^4 \ (^1\Sigma^+)$$

with 1σ, 2σ and 3σ corresponding to localized O $1s$, N_C $1s$ and N_T $1s$ respectively.

The Auger spectrum of free N_2O was analyzed already in 1976 by Connor et al. using restricted Hartree–Fock and limited configuration interaction wave functions coupled to the one-center model for Auger intensities [22]. These authors could grossly assign features to localization of orbitals and to the spread of singlet and triplet multiplet states.

The non-equivalent N atoms also make for ideal studies with coincidence spectroscopy. With studies including the dissociation of N_2O using electron–ion coincidences [23], site-specific fragmentation [24], multi ion–electron coincidences [25], and site-selective Auger electron spectra recorded using photoelectron-Auger electron coincidence spectroscopy (APECS) [26]. All of the mentioned coincidence studies were performed in the gas phase and to the best of our knowledge no APECS studies have to date been published on adsorbed N_2O.

Herein we present the first APECS study on adsorbed N_2O on Ni(111). This particular surface was chosen since the weak chemisorption leaves the molecular adsorbate intact [15]. Together with *ab initio* calculations we characterize the surface-adsorbate bond mechanism in detail.

2. Materials and methods

2.1. Samples and preparation

The Ni(111) crystal (99.995% MaTecK Gmbh) was cleaned with repeated cycles of argon sputtering (1.5 kV, 10 mA, $5 \cdot 10^{-6}$ mbar) for 5–10 min each followed by annealing to 1070 K for 3 min. The surface was then checked for contamination using X-ray photoelectron spectroscopy (XPS) revealing a clean surface with O $1s$ and C $1s$ contributions within the noise of a survey spectrum. After cooling the crystal using liquid helium, N_2O (5N, Messer) was dosed using a leak valve into the experimental chamber. The thermocouple readout during deposition was 31 K (with the temperature on the sample probably higher as discussed in the results below) with N_2O at a pressure of $1 \cdot 10^{-7}$ mbar. For the thick film a total of 100L N_2O was dosed and for the intermediate and monolayer films 5L was dosed prior to heating to desorb all but the desired thickness, details in the text below.

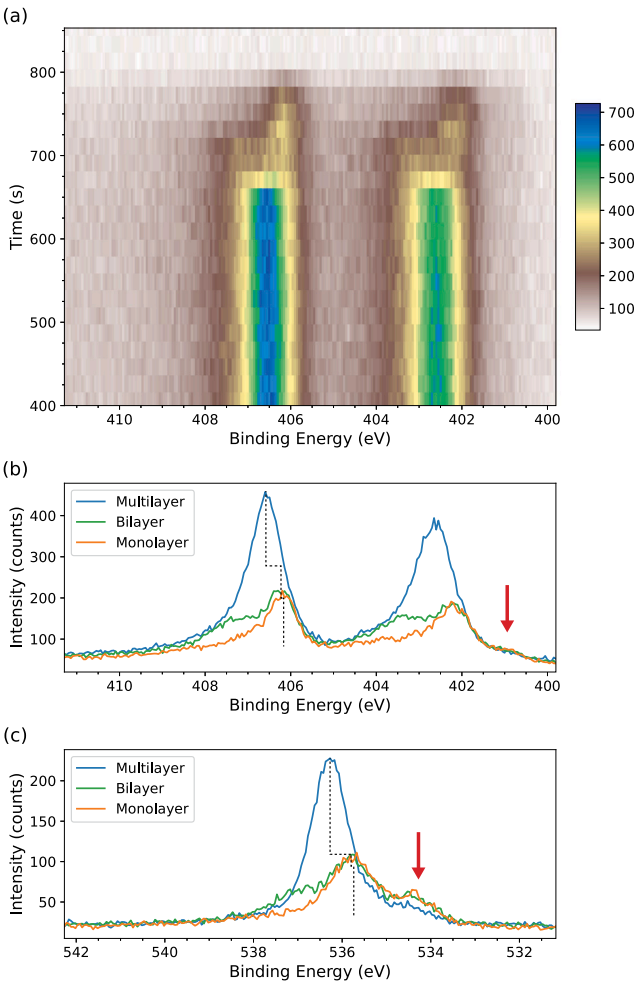

Fig. 1. (a) shows the evolution of the N $1s$ core level while heating the sample. At 650 s the thermocouple readout was 39 K and at 800 s 42 K with all molecules desorbed, further discussed in the text. The bottom two panels shows 3 typical spectra of N $1s$ (b) and O $1s$ (c) of multilayer, bilayer and monolayer coverage. With dashed lines highlighting the binding energy shifts of the different coverages and red arrows the binding energy of dissociated O and N.

2.2. Spectroscopic methods

The measurements were performed using the Coincidence Spectroscopy for Chemical Analysis (CoESCA) endstation [27] at the UE52-PGM beamline [28] at the BESSY II electron storage ring operated by the Helmholtz-Zentrum Berlin für Materialien und Energie.

For all measurements a photon energy of 700 eV was used and for the coincidence measurements an exit slit of 100 μm, resulting in a photon bandwidth of 100 meV. The CoESCA endstation is equipped with two angular resolving time-of-flight spectrometers (type ARTOF by Scienta Omicron). For the desorption and coincidence measurements the two ARTOFs were recording different kinetic energy regions. The N $1s$/N KVV coincidence measurements at all N_2O coverages and the O $1s$/O KVV coincidence measurements at monolayer N_2O coverage were done by measuring the Auger electrons with the ARTOF1 spectrometer (ARTOF10k) with a lens mode covering an energy window of 7% of the center kinetic energy and by measuring the photoelectrons with a ARTOF2 EW spectrometer with a lens mode covering an energy window of 4% of the center kinetic energy. The multilayer and bilayer N_2O O $1s$/O KVV coincidence measurements were performed during a second beamtime and in-between these sessions the ARTOF1 spectrometer was replaced with a second ARTOF2 EW, again using a 7% energy window. A consequence of addition of a second wide angle

Table 1
Summary of the coincidence statistics for the different APECS measurements, showing, number of true coincidence counts, the true to accidental ratio and the count rate. Note that the count rate is considerably larger for the multi- and bilayer O runs, this is from two different experiments where the experimental set-up was upgraded in-between as detailed in the experimental section.

	True counts	True/Acc	Countrate (s^{-1})
Nitrogen			
Multilayer	24 595	0.71	4.3
Bilayer	84 149	1.96	3.5
Monolayer	155 890	1.04	4.4
Oxygen			
Multilayer	84 582	0.56	15.7
Bilayer	64 735	0.85	12.2
Monolayer	57 182	1.13	1.7

spectrometer is a considerable increase in the coincidence count rate as seen in Table 1.

During a APECS measurement, events when both spectrometers record an electron within a given time window, are recorded as a coincidence event. This includes both true and accidental coincidences. Accidental coincidence events are when electrons from different ionization events hit the detectors in the same time window. The true events are extracted from the total coincidence counts by subtracting the accidental coincidences, as described in detail in [27,29]. In all coincidence spectra below, only the true coincidence events are plotted.

The statistics for the coincidence measurements are presented in Table 1. The binding energies were calibrated using the Fermi level of the Ni(111) crystal as a reference and the kinetic energies were calibrated using the Fermi level plus the work function on Ni(111), 5.23 eV [30]. For details on the APECS technique at the CoESCA station see [27,29,31,32].

2.3. Theoretical methods

Density functional theory (DFT) calculations were carried out using projector augmented-wave (PAW) formalism [33] as implemented in the Vienna *ab initio* simulation package (VASP) [34,35]. The revised Perdew–Burke–Ernzerhof (rPBE) [36] and Heyd–Scuseria–Ernzerhof (HSE06) [37] exchange–correlation functionals with the Grimme D3 correction [38] to weak disperse interactions were utilized to optimize the geometry and calculate electronic structure. Mostly the rPBE functional was used unless otherwise specified. The plane wave kinetic-energy cutoff of 450 eV was used. The first Brillouin zone was sampled by the Monkhorst–Pack scheme [39] with 12 × 12 × 1 k-points. The convergence tolerances of the force and electronic minimizations were 10^{-4} eV/Å and 10^{-6} eV, respectively. A vacuum region of > 10 Å was set to avoid artificial interactions between images. Atomic structures were visualized using The Visualization for Electronic and Structural Analysis (VESTA) software [40] and the ”vaspkit” code was employed for postprocessing the results [41].

In addition to solid state calculations we have carried out *ab initio* calculations on N_2O and N_2O-Ni using the MOLCAS program suite [42], with the purpose of having a theoretical characterization of the backdonation. We focused first on the electronic structure of the ground state considering a simple model, where for N_2O-Ni the internal geometry of the N_2O molecule was kept as it gas phase equilibrium geometry, whilst the distance between the N_T and the Ni atom was 1.87 Å. The calculations was addressed at the RASPT2 level of theory [43], together with the ANO-RCC-VQZP basis set. The design of the active space was carried with respect to energy convergence and occupation numbers. The active space finally used for N_2O was composed by six a_1 orbitals, one a_2 orbital, four b_1 and four b_2 orbitals. Such active space was chosen like $(6\sigma)(7\sigma)(2\pi)(3\pi)(4\pi)$ orbitals of N_2O and the $(3d)(4s)(4p_z)$ atomic orbitals of Ni (Fig. 3), totaling 22 electrons in 15 orbitals. The convergence of the wave-function was based on a state-average procedure considering a configuration interaction between the lowest 10 states.

For the calculations of the Auger transition intensities we firstly note that these are governed by two-electron Hamiltonian elements that couple to the continuum function of the outgoing Auger electron. As the precise determination of the Auger electron continuum function in the anisotropic molecular potential is a quite daunting task only a few methods have been put forward at this level of theory and applied for the smallest free molecules. Therefore a more practical approach adopted here is to consider the local nature of Auger transitions and use so-called one-center models [44,45], where two-electron coupling to the continuum is replaced by atomic continuum integrals weighted by the local on-atom atomic orbital expansion coefficients [46] of the involved (two) molecular orbitals (MOs) for the atom in question. Providing a quick inspection of the spectra, one can utilize an even simpler model based on orbital population, and only qualitatively consider the variation of the coupling to the continuum. In this view, combinations of orbital populations can guide the Auger spectrum even for surface adsorbates. It is notable that there are both singlet and triplet spin couplings for the two-hole Auger final states, but that a propensity rule [44,45] favors the singlets (owing, respectively, to constructive and destructive interference between Coulomb and exchange continuum integrals). Finally, we note that the two hole states are subject to ”Coulomb explosion” leading to dissociative final states and broad features, possibly except for one or two of the lowest lying final two-hole states [47]. It is to be noted that second quantization derived intensity expressions for Auger transitions between core ionized and double hole final states in a non-orthogonal basis contains many terms [48], but that the common Wentzel one-term ansatz [49] is still almost always assumed in actual calculations. That raises the question of which orbital basis is to be preferred. We have here in the below the presentation of the spectra using the one-center intensity model, assuming both ground and core hole optimized orbitals, bearing in mind that rather significant differences may arise.

3. Results and discussion

3.1. XPS and coverage

The N 1*s* core level photoelectron spectrum of N_2O consists of two contributions, one at higher binding energy from the N_C atom and one at lower binding energy from the N_T [11] . As can be seen in the multilayer spectra, blue spectrum in Fig. 1b, the contributions are well separated and the binding energy positions and peak widths fit well with earlier studies [16]. The multilayer O 1*s* primarily consists of one component as can be seen in Fig. 1c with a small contribution at lower binding energies that arises from dissociated O at the surface [3,20,29]. The presence of dissociated O also suggests a presence of dissociated N which could explain the shoulder seen at 401 eV binding energy for all coverages in the N 1*s* spectra in Fig. 1 [3,50]. The two dissociated species are marked with red arrows in Fig. 1. At minute coverages N_2O is known to dissociate at steps at vicinal Ni(755), a process that is terminated when step-sites are saturated with O [20]. The dissociation observed here occurs at defects on our Ni(111) crystal and the core level spectra suggest that it is in small quantities. As noted, the binding energy position of the dissociated N is well separated from those of N_2O [50]. The KLL Auger spectra from N_2 and N_2O will overlap in our kinetic energy region of interest; the main feature of N_2 Auger spectrum may be found around 360 eV kinetic energy [51] and being a minor contribution to the total spectrum and indistinguishable. This and the contribution to the O Auger spectrum are discussed in detail below.

In order to investigate the interaction between the substrate and the N_2O, thinner films were produced by heating the sample to control desorption. After exposing the cooled Ni surface to 5L of N_2O, it was slowly heated using resistive heating while simultaneously recording

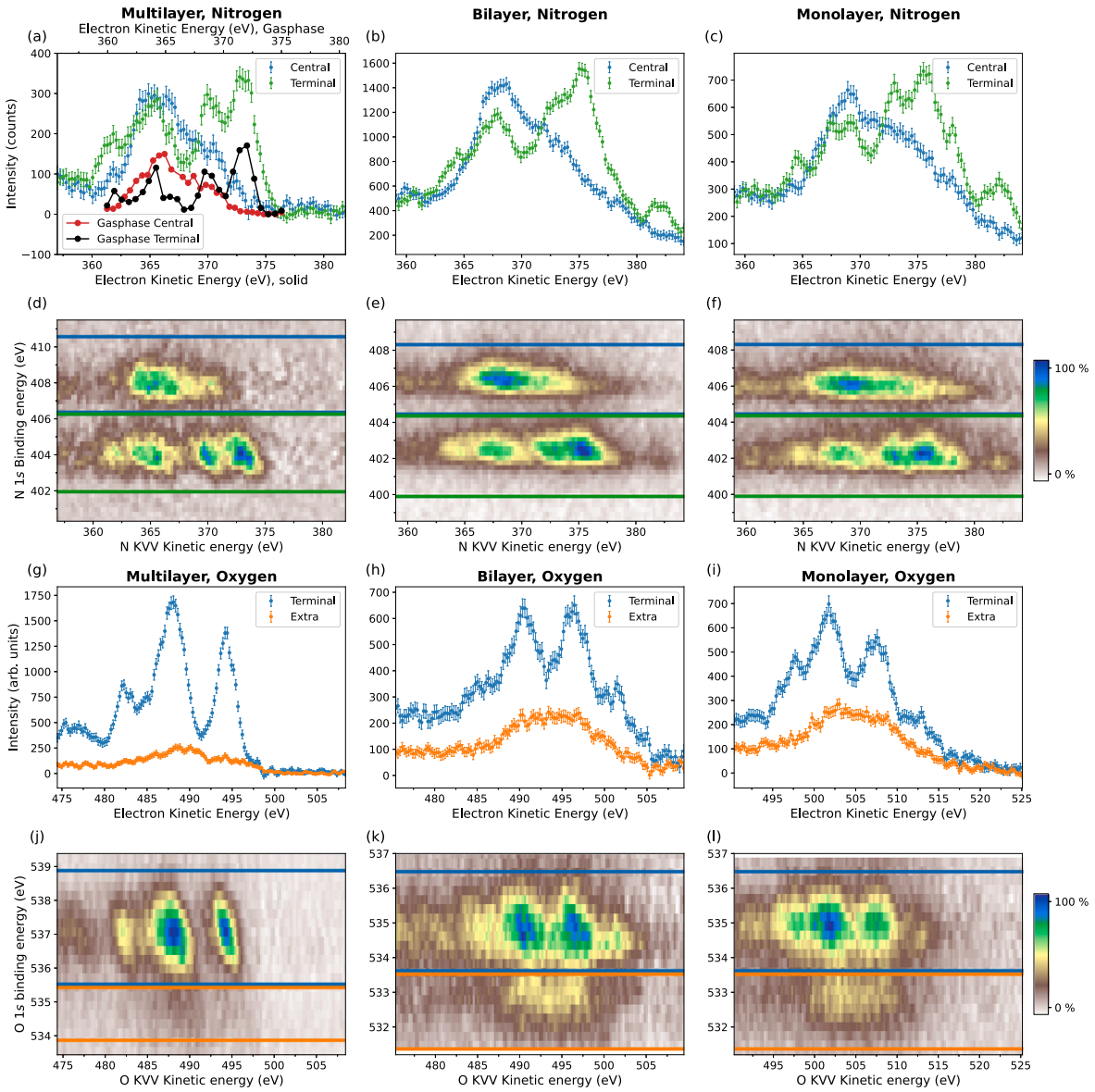

Fig. 2. Panels a–f show the N coincidence maps and integrated spectra from the regions marked with colored lines in the coincidences maps. Panel a also shows a comparison to the coincidence spectra from gas-phase N_2O, the gas-phase data is taken from Ref. [26], note the top energy axis for the gas-phase reference. Panels g–l shows the corresponding O coincidence data.

the N 1*s* and O 1*s* photoelectron spectra using the two ARTOF spectrometers. Monitoring the N 1*s* spectra while heating, as seen in Fig. 1a, shows a clear point of the multilayer desorption with a sharp decrease in the peak intensities followed by a small shift ($\Delta = 0.52$ eV) and the appearance of a doublet peak for each N atom, the green spectrum in the middle panel of Fig. 1. With further heating one peak of the doublet disappears with the other remaining unchanged, the orange spectrum in the middle panel of Fig. 1, until all molecules are desorbed and no N signal can be seen. The O 1*s* spectrum shows a similar trend as seen in the bottom panel of Fig. 1.

A similar behavior is discussed by Väterlein et al. [3] where their thermal desorption spectra revealed multilayer desorption at 70 K, monolayer desorption at 92 K and a third species which they attributed to a dilute monolayer that desorbed at 100 K containing 10% of a monolayer. They also claim no significant binding energy shift for the monolayer and dilute monolayer. This is similar to our results with three distinct steps in the desorption process but we observe a binding energy shift between the two lower coverage cases and that the low coverage case consists of 50% of the intermediate case. However, we observe this with significantly lower temperature read-out indicating that the actual sample temperature in our experiment is higher than the read-out, probably due to the location of the thermocouple. We assign the intermediate state with the doublet peak structure (green in Fig. 1) as bilayer coverage whereas the single peak structure (orange in Fig. 1) is assigned to monolayer coverage, with a molecular coverage of $\theta = 5/9$ determined from calculations as described below. This would follow a Frank–Van der Merwe layer-by-layer growth structure.

3.2. Auger-Photoelectron Coincidence Spectroscopy

3.2.1. Multilayer films

In Fig. 2d the N 1*s*/N KVV coincidence map of a multilayer N_2O film on Ni(111) can be seen. The map is dominated by two distinct intensity regions distributed in binding energy that are marked with blue (406–411 eV) and green (402–406 eV) lines. Looking at the binding energy positions for these regions the intensity comes from the two different N atoms in the molecule and they have seemingly different Auger spectra. By integrating the region around the binding energies for the two different N atoms the Auger spectra for each can be extracted.

These spectra can be seen in Fig. 2a where the blue and green spectra are the integrated region marked with the blue and green lines in the map below. The blue corresponds to N_C and the green to N_T. The N_T Auger spectrum contains more distinct features compared to the N_C. The Auger spectra of both N atoms are similar to that of gas-phase N_2O measured in coincidence by Bolognesi et al. [26] which is also plotted in Fig. 2a for comparison, note the separate kinetic energy axis for the gas phase spectra. The main features of the gas phase spectra are reproduced in the thick film albeit with a shift induced from the solid structure and by the substrate. The two energy axes are aligned so that the main Auger feature at 373.5 eV for both solid and gas end up at the same position in the figure. With these aligned it can be seen that other Auger feature also show some small shifts but are generally well reproduced.

Using a mean free path (λ) of 11 Å (calculated with the TPP-2M method [52]) for both photo- and Auger electrons (close to the same kinetic energy for this experiment) the effective mean free path for the APECS experiment can be calculated to 5.5 Å or about 2 monolayers [53]. Since the film is thicker than this, the APECS measurement is of pure solid N_2O and does not probe the interface with the Ni surface.

The O 1*s*/O KVV coincidence map of the multilayer film can be seen in Fig. 2j. It is dominated by 4 features in the 536–538 eV binding energy range, noticeably these exhibit a slight tilt. This correlation of the kinetic energies of the Auger- and photoelectron pairs can only be revealed in a coincidence measurement. While the well known energy sharing between an Auger and a photoelectron (e.g. [54]) leads to intensity stripes at constant kinetic energy sum, here we observe an opposite trend, where the stripes are rather at constant kinetic energy difference. The tilt is most apparent in the multilayer case and completely absent in the monolayer case (Fig. 2l). This could be explained by a change in the dielectric function with different film thicknesses resulting in different binding energies for spectra from different depths [55].

3.2.2. Bi- & monolayers

The bi- and monolayer coverages were produced by stopping the heating of a thick film (5L exposure) when the desired spectral features were observed and subsequently the sample was cooled down to base temperature again for the duration of the measurements. APECS measurements were then performed on these two coverages. The resulting APECS maps and integrated region spectra can be seen in Fig. 2 for N 1*s*/N KVV and O 1*s*/O KVV for the few- and monolayer coverages.

Comparing the N coincidence maps in Fig. 2 for the different coverages the shift seen in the XPS spectrum from the desorption is also seen in the Auger although much larger, $\approx$ 2.5 eV. Particularly the N_T Auger spectra are comparatively different from the multilayer and gas phase spectra. The monolayer spectrum contains sharp features whereas the bilayer case contains both the features of the monolayer interaction with the substrate and the interaction with the molecular layers above it. As discussed previously, the signal in the bilayer case is dominated by the top-most layers owing to the shallow information depth in APECS.

The O 1*s*/O KVV coincidence map, similar to the N 1*s*/N KVV case, contains two different binding energy separated Auger spectra where the one at high binding energy has a distinct structure similar to that seen in the N spectra. The Auger spectra from the 534–537 eV binding energy resemble those of the electron–ion coincidence gas phase Auger spectrum [24]. The low binding energy part contains a single broad peak in the Auger kinetic energy and binding energy region where we expect dissociated O to be present [3,20,29].

The most striking feature in the monolayer case is the intensity found above 380 eV kinetic energy for N_T. It is also present in the bilayer spectra but with lower intensity as expected since the signal from the monolayer is damped by the presence of the molecular layer on top of it and it is not observed in the thick film case (Fig. 2j).

3.3. Theory - N_2O Auger

The Auger coincidence spectra, Fig. 2, show some salient features spreading over an interval of about 15 eV in kinetic energy. It is clear that for both bi- and monolayer N_2O there is a shift of intensity towards higher kinetic energies for N_T compared to the N_C spectra. The former shows an additional weaker structure towards the high energy end for N_T not at all represented for N_C. It is notable that the N Auger spectrum of free N_2O [22], which is a composite of N_T and N_C transitions, show three main bands in this energy interval, but shifted towards lower kinetic energies by a few eV than the spectra in Fig. 2. The results of the RASSCF/PT2 calculations in terms of leading configuration and energy of the outer Auger states are given in Table 2. Here the energy of the outermost state ($2\pi^{-2}\ ^3\Sigma^-$) is used as a reference point. By inspecting the core separated spectra in Fig. 2d-f it is clear that the outermost band (at high Auger electron kinetic energies) of the composite N spectrum covering 0–6 eV is dominated by Auger transitions connecting to the N_T. The separated N_T spectrum shows two bands in this region. The computational assignment is here clear — the outermost of these two bands refers to terminally localized 2π and 7σ orbitals, while the inner one of the two also receives contributions from the more central N localized 1π orbital, n.b. in combination with 2π MO so generating the $1\pi^{-1}$, $2\pi^{-1}\ ^1\Pi$ and $^3\Pi$ eigenstates. We note, as is the general case for molecular valence Auger spectra, that there is a great deal of breakdown of the molecular orbital picture in analyzing the spectrum [47,56]. Thus only for the outer MOs (1π, 7σ, 2π) a one-to-one assignment can be made between two MOs and (spin-coupled) single configurational eigenstates. Here a division between inner–inner, inner–outer and outer–outer valence regions is appropriately based on the inclusion of the atomic 2s or 2p into the MOs. It is often the case that inner–inner valence states suffer a complete breakdown, the inner–outer a partial breakdown, while only the outer–outer valence states may receive an orbital assignment including only two MOs [47]. This means that both orbital localization and the breakdown effects come into play when analyzing the N_2O Auger spectrum. Thus going to lower Auger energies and the second, N_C, dominated broad band the breakdown effects become progressively more important.

3.3.1. Auger spectra of free N_2O

The ground state of free N_2O has populations of atomic 2*s* of +2.01 and +0.95 for N_T and N_C, respectively, whilst for the three 2*p* orbitals we have +3.33 and +2.77. Besides, in Tables 3 and 4 we can also see the expansion coefficients of the valence MOs, by atomic center. We note a rather strong shift of charge towards the end atoms at the expense of charge for N_T - this complies with the fact that the overall intensity of the Auger spectrum is stronger for N_T than for N_C for both the bi- and monolayer cases. The shift of intensity towards lower energies for N_T compared to N_C can also be qualitatively understood from this table as one roughly can divide the Auger spectrum into 2*p*2*p* outer valence, 2*s*2*p* outer–inner valence and 2*s*2*s* inner valence regimes [47], going from high to low kinetic energies. Thus 2*p* dominance of an atom tend to give intensity of the upper region. This is further accentuated by the atomic coupling to the continuum, with integrals that are significantly stronger for 2*p*2*p* than for 2*s*2*p* or 2*s*2*s* two-holes states of the N atom [46]. Thus a rough inspection of atomic charges indicates that N_T spectra are stronger in total than N_C spectra and that the N_T spectra are shifted towards lower kinetic energies.

The MO populations will also guide the intensities in these regions. It is clear that the 6σ, 1π, 7σ, 2π orbitals are well separated from remaining orbitals (a predicted 16 eV gap), and thus well define the ”outer valence”. Their energy positions also comply well with the solid state density of states analysis given in Fig. 8. That they dominate the low kinetic energy parts is also proven by the MCSCF analysis of total N_2O two-hole state energies in Table 2. As we see from this table all states in a 7 eV span derive from combinations of the four outer valence orbitals. Especially, the $2\pi^{-2}\ ^1\Delta$ and $2\pi^{-1}7\sigma^{-1}\ ^1\Pi$ states in the lower

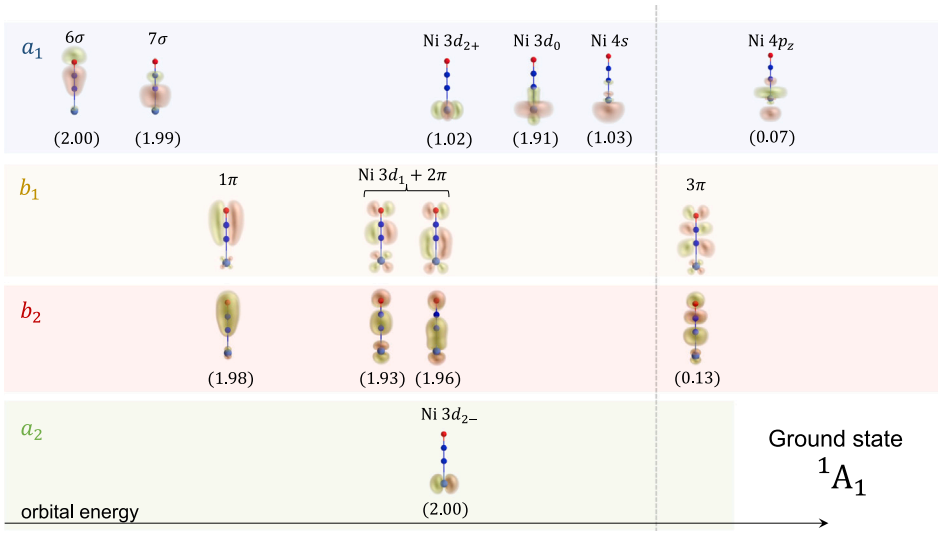

Fig. 3. Diagram of the active space used for describing the ground state of the N_2O+Ni idealized structure. The MOs are disposed according to the symmetry components of the C_{2v} point group, and they are arranged by orbital energy from left to right. The vertical dashed line divides the occupied orbitals (left) from the unoccupied orbitals (right). Numbers in parenthesis denote natural occupation numbers.

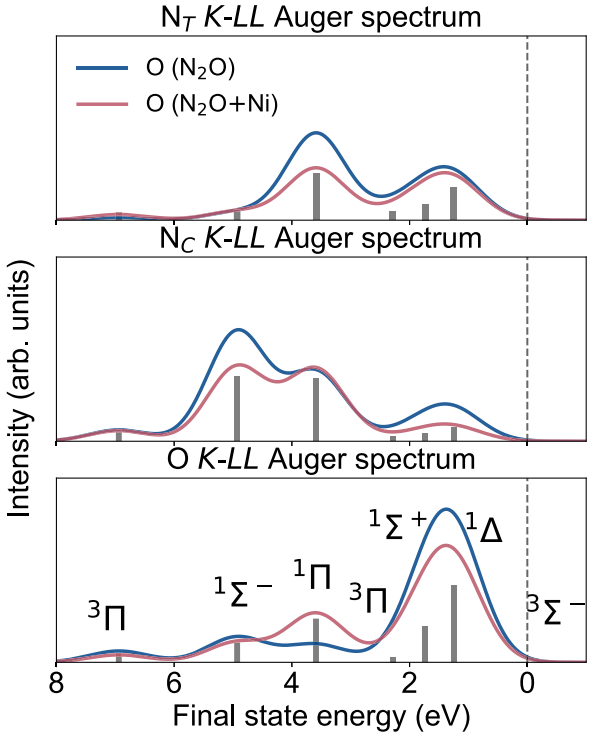

Fig. 4. Theoretical Auger spectrum obtained with the one-center approximation for both single N_2O and N_2O+Ni systems, calculated at the N_T K-edge (top), N_C K-edge (middle) and O K-edge (bottom). The energies in the horizontal axis are calculated using the $^3\Sigma^-$ state as the reference. The molecular symbols in the bottom plot are the same for the other graphics.

Table 2
Relative energies, in eV, of the triplet and singlet Auger states of N_2O. The reference value corresponds to the ground state $^3\Sigma^-$ of N_2O^{2+}.

State	Config.	ΔE (eV)
$^3\Sigma^-$	$2\pi^{-2}$	0.00
$^1\Delta$	$2\pi^{-2}$	1.25
$^1\Sigma^+$	$2\pi^{-2}$	1.73
$^3\Pi$	$7\sigma^{-1}2\pi^{-1}$	2.29
$^1\Pi$	$7\sigma^{-1}2\pi^{-1}$	3.59
$^1\Sigma^-$	$1\pi^{-1}2\pi^{-1}$	4.93
$^3\Delta$	$1\pi^{-1}2\pi^{-1}$	5.44
$^3\Sigma^+$	$1\pi^{-1}2\pi^{-1}$	5.58
$^3\Sigma^-$	$1\pi^{-1}2\pi^{-1}$	5.80
$^3\Pi$	$6\sigma^{-1}2\pi^{-1}$	6.94

Table 3
N_2O MO coefficients for the valence σ orbitals.

sym. adpat. basis	7σ	6σ	5σ	4σ
N_T 1s	−0.0347	+0.0101	+0.0074	−0.0066
N_T 2s	−0.7187	+0.3908	−0.5884	+0.2890
N_T 2p_z	+0.5775	−0.0840	−0.2517	+0.1269
N_T 1s	+0.0062	+0.0118	+0.0228	−0.0613
N_T 2s	+0.2044	−0.3548	−0.1563	+0.3948
N_T 2p_z	−0.2807	−0.1808	+0.2801	+0.0533
O 1s	+0.0038	+0.0124	−0.0021	−0.0096
O 2s	+0.1256	+0.5912	+0.5351	+0.5775
O 2p_z	+0.2717	+0.5690	−0.1261	−0.1877

5 eV region. We note from Tables 3 and 4 that both 7σ and 2π orbitals have strong N_T 2p contributions, and the strong composite N_T band at 370–375 eV should be assigned to these two states. Correspondingly the N_C 2p contributions to these orbitals are substantially smaller, explaining the much lower intensity in this region. Going further down in the spectra, into the 2s2p region, there is a rather mixed representation of N_T and N_C in terms of atomic orbital composition, and we also observe rather smeared out "look-alike" features in the two spectra. The orbital characterization is also becoming less relevant due to the above mentioned MO breakdown effects. Furthermore, analyzing the role of the surface, see below, it is clearly the outer 2p2p region which matters most.

3.3.2. *Auger spectrum of N_2O-Ni*

Going from free to surface adsorbed N_2O the most salient spectral feature in the Auger spectra is thus the addition of a structure at 385 eV kinetic energy appearing in the N_T spectrum but not for N_C. Evidence that this feature relates to backdonation is reflected in the electronic structure of the ground state. Therefore, in order to have a meaningful description of the backdonation, we have considered an idealized model of a system composed of one molecule of N_2O plus a single Ni atom, all disposed in a linear structure.

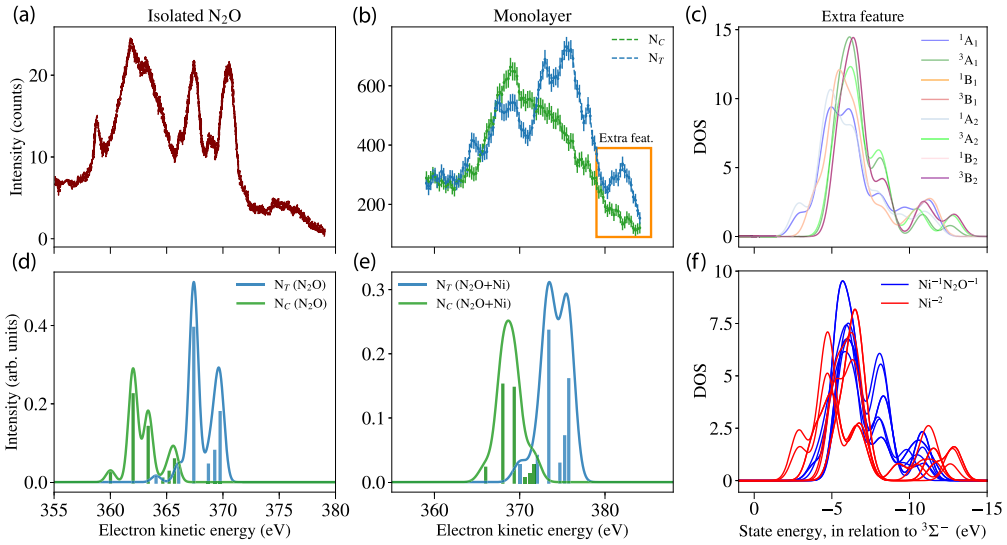

Fig. 5. (a) Experimental Auger spectrum for isolated N_2O, as a function of the electron kinetic energy, in eV, from Ref. [22]. (b) Experimental Auger spectrum for the monolayer, as a function of the electron kinetic energy, in eV. (c) Detailed composition of the extra structure at 380–385 eV in panel (b), showing density of doubly charge states with energies below $^3\Sigma^-$, colored according to the electronic wave function symmetry (C_{2v} point group). The spectral curves are obtained from a straight summation of the density of states. (d) Theoretical Auger spectrum obtained for isolated N_2O, corresponding to the main structures of the experimental signal. Bars represent relative intensities according to the one-center approximation. (e) Theoretical Auger spectrum obtained for N_2O+Ni, corresponding to the main structures of the experimental signal. Bars represent relative intensities according to the one-center approximation. (f) Same as panel c, but the density of doubly charge states with energies below $^3\Sigma^-$ is here divided into doubly ionized Ni (red) and singly ionized Ni plus singly ionized N_2O (blue). Note that, in contrast to panel c.

Table 4
N_2O MO coefficients for the valence π orbitals. The π MOs are x/y-doubly degenerate (b_1/b_2).

sym. adpat. basis	2π	1π
N_T $2p_x/2p_y$	−0.5659	+0.3449
N_T $2p_x/2p_y$	−0.2162	+0.5742
O $2p_x/2p_y$	+0.7743	+0.4849

Table 5
N_2O+Ni MO coefficients for the valence σ orbitals.

sym. adpat. basis	N_2O 7σ	N_2O 6σ	Ni $3d_{2+}$	Ni $3d_0$
N_T $1s$	−0.048	−0.020	0.000	0.030
N_T $2s$	−0.799	−0.006	0.000	0.271
N_T $2p_z$	+0.461	+0.069	0.000	−0.045
N_T $1s$	+0.027	+0.059	0.000	−0.021
N_T $2s$	+0.430	−0.214	0.000	−0.167
N_T $2p_z$	−0.222	−0.363	0.000	0.088
O $1s$	+0.000	+0.015	0.000	−0.001
O $2s$	−0.036	+0.039	0.000	−0.003
O $2p_z$	+0.028	+0.657	0.000	−0.020
Ni $3d_{2+}$	+0.000	+0.000	0.997	+0.000
Ni $3d_0$	−0.138	−0.015	+0.000	−0.929
Ni $4s$	−0.189	−0.037	+0.000	+0.086

Table 6
N_2O+Ni MO coefficients for the valence π orbitals. The π MOs are x/y-doubly degenerate (b_1/b_2).

sym. adpat. basis	N_2O $2\pi_{x/y}$	N_2O $1\pi_{x/y}$	Ni $3d_{1+/-}$
N_T $2p_{x/y}$	+0.628	+0.386	+0.011
N_T $2p_{x/y}$	+0.034	+0.609	+0.002
O $2p_{x/y}$	−0.706	+0.412	+0.005
Ni $3d_{1+/-}$	−0.044	−0.030	−0.995

Within this linear model, we can understand the effect of the nickel atom as (i) the influence on the Auger transitions corresponding to the states of isolated N_2O and (ii) the introduction of new transitions (mainly due to the backbonding). For the first part, a partial Auger spectra was calculated based on the one-center approximation (Fig. 4). Here we look at the same final states of single N_2O, and we report the spectra calculated for N_2O and for N_2O+Ni. The assignments of the final states respect the labels of single N_2O molecule, also shown in Table 2. It is worth pointing out that the lowest-lying $^3\Sigma^-$ state has no intensities in the one-center approximation. The reason is that the Coulomb and exchange integrals cancel each other out in this case. For all three core-holes we observe three main bands in this energy interval, the first corresponding to the $^1\Delta$ plus $^1\Sigma^+$ states, and the second and third related to the $^1\Pi$ and $^1\Sigma^-$ states. The triplet Π states have lower intensities as discussed above. Although it can be considered as a marginal effect, the presence of the nickel atom change the relative intensity of these transitions as a response to the changes on the MO coefficients, when compared to the isolated N_2O (Tables 5 and 6).

Our interpretation of the overall spectra is that (i) the most intense peaks in the experimental spectrum (taking N_T, for instance, the peaks from 365–375 eV) correspond to the transitions on N_2O, principally the ones linked to the singlet states as discussed above, and (ii) the extra structure at higher kinetic energies corresponds to states involving ionization of the Nickel atom. We thus understand that this is a consequence of the latter effect of the nickel atom (the introduction of new transitions). This interpretation is supported by our RASPT2 calculations for the doubly charged N_2O+Ni. In fact, the lowest-lying doubly charged state lies below the $^3\Sigma^-$ state by more than 13 eV, and corresponds to a double ionization of the nickel atom. With our active space, more than 300 roots were found in this interval, below the $^3\Sigma^-$, which was set as the reference energy. Besides, the density of states shows a broad peak between −4 eV and −10 eV, which is in a very good agreement with the experimental value of the extra structure (Fig. 5).

The local nature of the Auger transitions suggests that the doubly ionized atomic nickel states have very low intensities, for they would involve non-local electron decays. On the other hand, those states involving singly ionization of the nickel atom together with singly ionization of the N_2O molecule would have larger intensities, although smaller than the main peaks. From Mulliken charge analysis, the states were divided into the ones involving doubly charged Ni (Ni+2) and the ones corresponding to singly ionized Ni plus singly ionized N_2O (Fig. 5f). The blue solid lines stand for the states that would provide more intense Auger signals, in comparison to the red line states. We

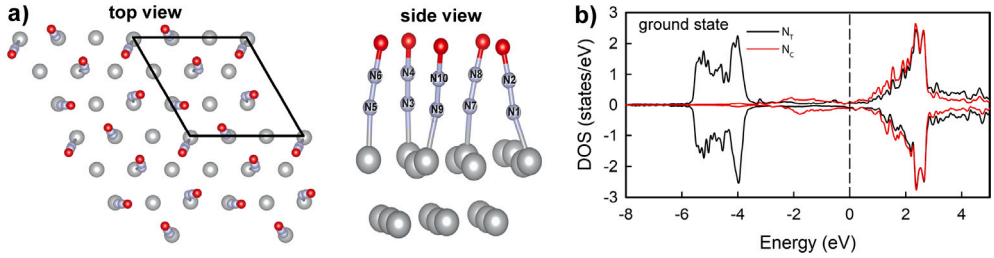

Fig. 6. Equilibrium geometry (a) and densities of states (b) of monolayer N_2O on Ni(111).

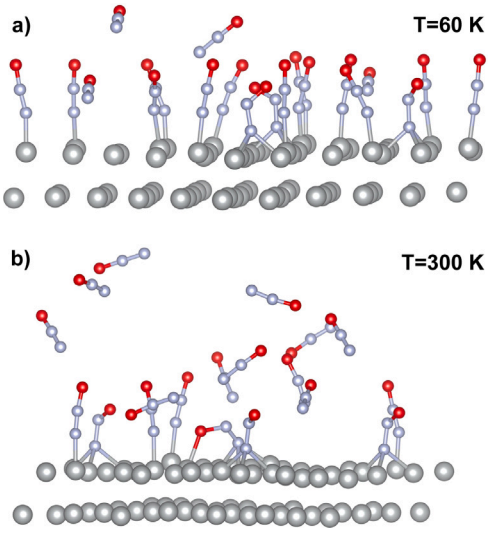

Fig. 7. Snapshots of N_2O monolayer on Ni(111) after 3 ps of the AIMD simulation at 60 (top panel) and 300 K (bottom panel) within NVT thermostat and a time step of 1 fs.

noticed that the band denoted by the blue line is roughly centered between −5 eV and −8 eV, which means 7 to 10 eV below the most intense $^1\Delta$ peak and agrees well with the experimental N_T spectrum. In Tables 5 and 6 we show the coefficients of the Ni 3*d* atomic orbitals in the outer valence MOs. The Ni $3d_0$ orbital in fact interacts with the 2*s* orbital of the N_T. That led us to conclude that the extra peak is built up principally of transitions involving Ni $3d_0^{-1}$ plus N_2O $2\pi^{-1}$. Furthermore, we can also use the same argument to explain why this structure cannot be clearly observed in the N_C spectrum.

3.3.3. Adsorption geometry

To examine the monolayer electronic structure we have made *ab initio* molecular dynamics simulations (AIMD) of the monolayer and density of state calculations of isolated and adsorbed N_2O. The equilibrium geometry at 0 K revealed a 3 × 3 overlayer structure (5 N_2O molecules per unit cell) with N_T closest to the surface on-top of the Ni atoms as seen in Fig. 6. The molecules demonstrate nearly the same preferable orientation as in the case of a single molecule on-top of Ni (discussed below) with some small bending. Thus reproduce the single molecule on Ni(111) by other authors [57]. In the adsorbed monolayer, the HOMO (which is contributed only by the N_T atoms bonded with the surface) is located between −5.8 and −3.8 eV and LUMO (contributed by both atoms) is between 1 and 3 eV.

To reveal the geometry of N_2O monolayer on the Ni(111) surface at finite temperature, we employed *ab-initio* molecular dynamics simulations (Fig. 7) at 60 and 300 K within NVT thermostat and a time step of 1 fs. It was found that at 60 K, part of the molecules are desorbed from the surface, while some of them change their positions from top to hcp/fcc and demonstrate some bending compared to the molecules adsorbed in the on-top position. At 300 K, we found that the number of desorbed molecules increased while the diversity in the geometries of adsorbed molecules became greater. For example, some molecules are adsorbed in a "lying down" geometry by binding both O and N atoms with Ni(111).

3.3.4. Density of states analysis

To investigate the density of states (DOS) in different bonding configurations we compare the isolated molecule to those adsorbed on-top and in a lying-down configuration. Fig. 8 from top to bottom demonstrates DOS of isolated N_2O, N_2O adsorbed in top position (lowest in energy without taking into account ZPE, zero-point energy, and entropy factors), and in lying down position with N_2O adsorbed by O (top) and N (hcp) which is the second in energy, but only predicted to be 0.05 eV higher compared to the top standing N_2O. We thus have two bonding situations that give very different DOS and therefore Auger spectra. Here we clearly notice states corresponding to the three uppermost occupied orbitals - 1π, 7σ, 2π - while above the 2π there is a HOMO-LUMO gap to the unoccupied 3π orbital. Going upwards in energy we see a gap to the higher lying orbitals, in a region represented by the breakdown effects according to Table 2. This plot thus represents a one-particle interpretation of the ionization spectrum of N_2O. The energy levels and localization, e.g. with the N_T localization of the two uppermost states, are in accordance with the Hartree–Fock (HF) analysis present in Table 5. The up and down plots represent spin-up and spin-down DOS. They are indeed equal for free N_2O as expected for a closed shell molecule. That result is also comparable well with the Hartree–Fock results for free N_2O, and is not surprising as Koopmans theorem (HF) and Janaks theorem (DFT) both equalize orbital energies with ionization potentials to a large degree of accuracy. For isolated molecules, it is thus quite clear that HOMO is localized on N_T, while LUMO is localized on both N atoms. Adsorption leads to interaction with the Ni(111) surface and as a result prominent shift of states to lower energies caused by electron transfer from Ni to the molecule. At the top position, HOMO is at −4.4 eV and LUMO is broadened between 1.5 and 4.4 eV due to proximity-induced effects. One can also see small but non-zero spin polarization of N_2O states.

The electronic structure of N_2O adsorbed in the complex configuration reveals a significant broadening of orbitals and spin polarization resulting from stronger interaction with the Ni(111) surface. This also can be confirmed by charge transfer analyzed by the Bader approach. The isolated N_2O reveals that the O atom gains 0.32e from the N_C part. Adsorption in the top position keeps the charge of O the same as in the isolated molecule while N gain 0.2e transferred from Ni(111). Complex adsorption leads to significant charge transfer from the surface to both N and O parts. For instance, O gains additionally 0.24 e as compared to isolated N_2O, while 0.53 e is transferred from the metal surface to N. This results in significant induced spin polarization of the molecule as demonstrated in DOS.

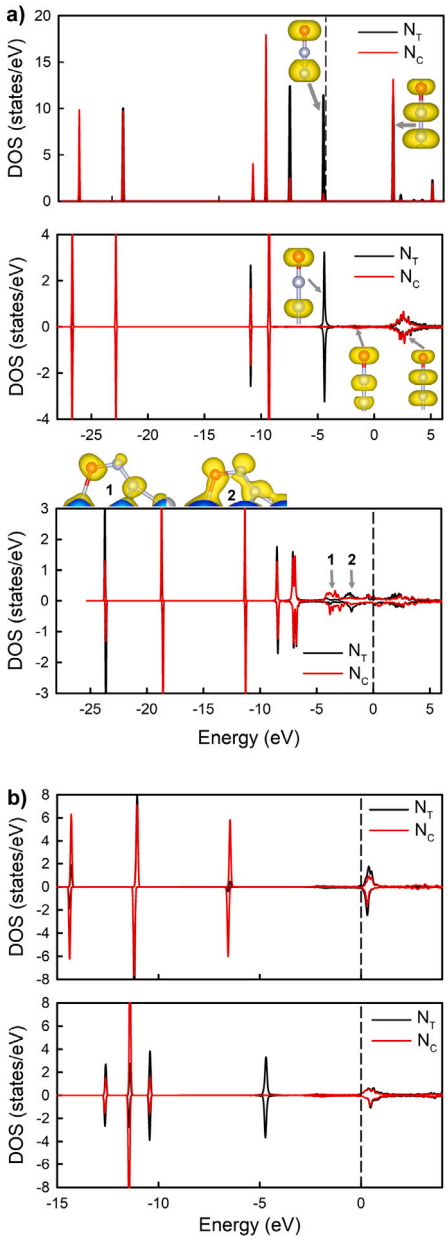

Fig. 8. (a) DOS of isolated N_2O (top), N_2O adsorbed in top position (middle) and N_2O adsorbed in lying down position (bottom). (b) Core ionized (N_T or N_C) N_2O density of states, where the core hole potential is represented by the equivalent core (Z+1) approximation (top panel core ionized on N_T and bottom panel on N_C). The Fermi level is set to 0 eV.

The DOS results indicate a shifted N_2O structure but with an additional broad structure appearing a few eV above the Fermi surface, replacing the LUMO level of free N_2O. This structure represents the surface to N_2O (3d- π^*) backbonding situation with the broad feature related to a splitting of the 3d band of Nickel by the N_2O bonding. Here we see that the free N_2O DOS results are very much compromised for the HOMO and LUMO levels, showing neither the preserved N_2O structure nor the 3d- π^* backbonding indicated by the standing up N_2O case in the middle panel of Fig. 8a.

Finally, in Fig. 8b we show the case of standing N_2O on the surface for core ionized (N_T or N_C) N_2O density of states, where the core hole potential is represented by the equivalent core (Z+1) approximation. As the core ionized state (CS) is the initial state of the Auger transition it can be relevant to compare it with the ground state results — here one sees that N_2O orbital structure is only minorly varied but that the 3d- π^* backbonding band complex is significantly stabilized in energy.

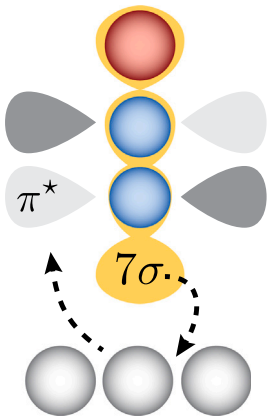

Fig. 9. Schematic view of the backdonation.

3.4. Blyholder or not

So considering the standing position it seems that the excess intensity in the high kinetic energy part of the Auger spectrum of the N_T atom (in comparison with the N_C atom) is due to charge transfer from metal to the $\pi^\star$ of the N_T atom. This is similar to the Blyholder back–donation model for CO / N_2 on transition metals, thus that in the ground state, there is back donation from metal 3*d* to the (otherwise empty) LUMO on the N atoms, something that strengthens the bonding of the adsorbate to the surface [21,58]. This back-donation has also been suggested by Kiss et al. for the N_2O on Pt(111) system [59] and from DFT analysis on N_2O on Fe-doped graphene [60].

The kinetic energy position of this extra intensity has been observed of N_2O in the gas phase both as a shake-up from core ionization [61] and resonant Auger [62]. In Fig. 9 we present backdonation into the LUMO from the nickel surface and the donation from the 7σ lone pair orbital of the N_T. This explains the chemisorbing nature of the N_2O/Ni(111) interaction and the extra intensity seen in APECS at high kinetic energy for the thin coverages that is not present in the multilayer film.

As indicated by the density of states analysis there is a broad extra structure around the Fermi level that can be interpreted as due to a N_2O (3d- π^*) backbonding situation. It is also possible to gain insight into the backdonation in the ground electronic structure from the idealized model considered above comprising a system composed of one molecule of N_2O plus a single Ni atom, all disposed in a linear structure, see further information in the computational section. Direct analysis of the Mulliken charges of the ground state indicates a slight total charge transfer from the Ni atom to the N_2O molecule. In fact, the total atomic charge on Ni is −0.05, and the charges of the N_T, N_C and O atoms are, respectively, −0.27, +0.78 and −0.47. By large this agrees well with the analysis of the DOS in Fig. 8. When considering the electronic charge occupying only the 3*d* and 4*s* atomic orbitals of Ni we obtained −9.59, against the expected −10 for the isolated Ni. On top of that, the occupation number of the orbitals also presents valuable information on the backdonation. First, the sum of the MO coefficients squared associated with Ni atomic orbitals of the orbital labeled as 7σ - occupation number 1.99 - is 0.07, which is a way of quantifying the hybridization of the 7σ orbital. Besides, the hybridization between the N_2O LUMO orbital (3π) and the 3*d*4*s* atomic orbitals of Ni produces a 0.13 population on the 3π orbital (second and third lines of Fig. 3), thus supporting the notion of a 3d- π^* backbonding.

4. Conclusions

APECS represents an experimental method where backdonation in surface–adsorbate bond may be directly measured. Additionally since we are able to distinguish the Auger spectra from chemically nonequivalent atoms, we can in cases when those are well separated determine which orbital at which atom receives the backdonated electron density.

We have compared multilayer, bilayer and monolayer coverage of N_2O on a Ni(111) surface where the multilayer film in many regards is similar to a kinetic energy shifted and broadened gas-phase spectra and we can see that the monolayer contains features not found in the gas-phase. For the N coincidences this new intensity feature arises from an interaction with the nickel substrate whereas in the O case the spectrum is not dependent on coverage. The observed behavior is explained with calculations that demonstrate that the N_2O is standing up with the N_T closest to the surface with a surface bond built up from donation and backdonation of electron density involving the Ni surface and the N_T atom.

The APECS methodology outlined here suggests that the method should be applied to problems in catalysis where small molecules interact with a substrate to make a detailed assessment of how they interact. In the present case for instance, we could identify the decomposition products and differentiate them from intact species. The present work also illustrates the insight into the electronic structure and dynamics of the surface adsorption gained by combining APECS and theoretical analysis — solid state and quantum *ab initio*.

CRediT authorship contribution statement

Fredrik O.L. Johansson: Writing – review & editing, Writing – original draft, Visualization, Methodology, Investigation, Formal analysis, Conceptualization. **Lucas M. Cornetta:** Writing – review & editing, Writing – original draft, Visualization, Investigation, Formal analysis. **Elin Berggren:** Writing – review & editing, Investigation. **Artem Kuklin:** Writing – original draft, Visualization, Investigation, Formal analysis. **Yi-Chen Weng:** Writing – review & editing, Investigation. **Swarnshikha Sinha:** Writing – review & editing, Investigation. **Danilo Kühn:** Writing – review & editing, Methodology, Investigation. **Alexander Föhlisch:** Writing – review & editing, Methodology, Investigation. **Hans Ågren:** Writing – review & editing, Writing – original draft, Methodology, Investigation, Formal analysis. **Andreas Lindblad:** Writing – review & editing, Writing – original draft, Supervision, Investigation, Formal analysis, Conceptualization.

Declaration of competing interest

The authors declare that they have no known competing financial interests or personal relationships that could have appeared to influence the work reported in this paper.

Data availability

Data will be made available on request.

Acknowledgments

F.O.L.J acknowledges support from the Swedish Research Council (Grant 2020-06409). L.M.C acknowledges the Brazilian funding agency FAPESP, under processes nr. 2020/04822-9 and 2021/06527-7. A.K. acknowledges Olle Engkvist Byggmästare Foundation for the support under contract no. 212-0178. We thank the Helmholtz-Zentrum Berlin für Materialien und Energie for the allocation of synchrotron radiation beamtime. The authors also acknowledge the Swedish National Infrastructure for Computing (NAISS 2023-3-40 and NAISS 2024-5-73) at the National Supercomputer Centre of Linköping University (Sweden) partially funded by the Swedish Research Council through grant agreements no. 2022-06725 and no. 2018–05973.

References

[1] G. Myhre, D. Shindell, F. Bréon, W. Collins, J. Fuglestvedt, J. Huang, D. Koch, J. Lamarque, D. Lee, B. Mendoza, et al., Climate Change 2013: The Physical Science Basis. Contribution of Working Group I to the Fifth Assessment Report of the Intergovernmental Panel on Climate Change, Cambridge University Press, Cambridge, UK, 2013.

[2] A. Ravishankara, J.S. Daniel, R.W. Portmann, Nitrous oxide (N_2O): The dominant ozone-depleting substance emitted in the 21st century, Science 326 (5949) (2009) 123–125.

[3] P. Väterlein, T. Krause, M. Bäßler, R. Fink, E. Umbach, J. Taborski, V. Wüstenhagen, W. Wurth, Adsorption-induced bending of a triatomic molecule: Near-edge X-Ray absorption fine-structure spectroscopy investigation of N_2O adsorbed on different Ni(111) surfaces, Phys. Rev. Lett. 76 (25) (1996) 4749.

[4] P. Glarborg, J.E. Johnsson, K. Dam-Johansen, Kinetics of homogeneous nitrous oxide decomposition, Combust. Flame 99 (3–4) (1994) 523–532.

[5] W. Qu, C. Wang, P. Wang, Y. Shen, J. He, D. Zhang, Insights into reaction pathway induced by d orbital occupancy on cobalt supported boron nitride for N_2O catalytic decomposition, Appl. Surf. Sci. (2023) 157792.

[6] M.D. Esrafili, H. Janebi, P. Mousavian, Single al atom anchored on defective MoS_2: An efficient catalytic site for reduction of greenhouse N_2O gas by CO or C_2H_4 molecules, Appl. Surf. Sci. 569 (2021) 151001.

[7] S.K. Hoekman, Review of nitrous oxide (N_2O) emissions from motor vehicles, SAE Int. J. Fuels Lubricants 13 (1) (2020) 79–98.

[8] Y.-K. Park, B.-S. Kim, Catalytic removal of nitrogen oxides (NO, NO_2, N_2O) from ammonia-fueled combustion exhaust: A review of applicable technologies, Chem. Eng. J. 461 (2023) 141958.

[9] D. Cui, S. Wu, T. Li, Y. Zhang, S.J. Yoon, Y.-S. Bae, B. Park, Y. Wu, R. Xiao, A novel fluidized-bed-electrode solid-oxide-fuel-cell reactor for N_2O catalytic decomposition, Chem. Eng. J. 466 (2023) 143123.

[10] G. Wight, C. Brion, K-shell energy loss spectra of 2.5 keV electrons in CO_2 and N_2O, J. Electron Spectrosc. Relat. Phenom. 3 (3) (1974) 191–205.

[11] M. Schmidbauer, A. Kilcoyne, K. Randall, J. Feldhaus, A.M. Bradshaw, M. Braunstein, V. McKoy, Angle-resolved photoelectron spectroscopy of the core levels of N_2O, J. Chem. Phys. 94 (8) (1991) 5299–5305.

[12] R. Lucchese, J. Söderström, T. Tanaka, M. Hoshino, M. Kitajima, H. Tanaka, A. De Fanis, J.-E. Rubensson, K. Ueda, Vibrationally resolved partial cross sections and asymmetry parameters for nitrogen K-shell photoionization of the N_2O molecule, Phys. Rev. A 76 (1) (2007) 012506.

[13] M.N. Piancastelli, D. Céolin, O. Travnikova, Z. Bao, M. Hoshino, T. Tanaka, H. Kato, H. Tanaka, J. Harries, Y. Tamenori, et al., A high-resolution study of resonant Auger decay processes in N_2O after core electron excitation from terminal nitrogen, central nitrogen and oxygen atoms to the 3π LUMO, J. Phys. B: At. Mol. Opt. Phys. 40 (17) (2007) 3357.

[14] S. Tada, M. Yokoyama, R. Kikuchi, T. Haneda, H. Kameyama, N_2O pulse titration of Ni/α-Al2O3 catalysts: A new technique applicable to nickel surface-area determination of nickel-based catalysts, J. Phys. Chem. C 117 (28) (2013) 14652–14658.

[15] A. Zeigarnik, Adsorption and reactions of N_2O on transition metal surfaces, Kinet. Catal. 44 (2) (2003) 233–246.

[16] C. Brundle, XPS and UPS studies of the interaction of nitrogen-containing molecules with nickel: The use of binding energy patterns and relative intensities to diagnose surface species, J. Vac. Sci. Technol. 13 (1) (1976) 301–309.

[17] T. Wu, X. Wang, Z. Jiao, H. Luo, P. Zhu, Structure of N_2O monolayer on Ag surface, Vacuum 101 (2014) 399–402.

[18] T. Wu, P. Zhu, H. Luo, X. Wang, The characteristics of self-assemble N_2O monolayer, Phys. Lett. A 374 (34) (2010) 3460–3463.

[19] R. Sau, J.B. Hudson, Decomposition of N_2O on Ni(110), J. Vac. Sci. Technol. 18 (2) (1981) 607–610.

[20] C. Kodama, H. Orita, H. Nozoye, Peculiar decomposition behavior of N_2O on Ni (755), Appl. Surf. Sci. 121 (1997) 579–582.

[21] H. Aizawa, S. Tsuneyuki, First-principles study of CO bonding to Pt(111): Validity of the Blyholder model, Surf. Sci. 399 (2–3) (1998) L364–L370.

[22] J. Connor, I. Hillier, J. Kendrick, M. Barber, A. Barrie, An experimental and theoretical study of the Auger spectrum of nitrous oxide, J. Chem. Phys. 64 (8) (1976) 3325–3329.

[23] L. Ferrand-Tanaka, M. Simon, R. Thissen, M. Lavollée, P. Morin, New results on core excited N_2O obtained by electron–ion coincidence spectroscopya, Rev. Sci. Instrum. 67 (2) (1996) 358–364.

[24] R. Murphy, W. Eberhardt, Site specific fragmentation in molecules: Auger-electron ion coincidence studies on N_2O, J. Chem. Phys. 89 (7) (1988) 4054–4057.

[25] D. Hanson, C. Ma, K. Lee, D. Lapiano-Smith, D. Kim, Single-event, energy-resolved, Auger–electron, multiple-ion coincidence mass spectroscopy, J. Chem. Phys. 93 (12) (1990) 9200–9202.

[26] P. Bolognesi, M. Coreno, L. Avaldi, L. Storchi, F. Tarantelli, Site-selected Auger electron spectroscopy of N_2O, J. Chem. Phys. 125 (5) (2006) 054306.

[27] T. Leitner, A. Born, I. Bidermane, R. Ovsyannikov, F. Johansson, Y. Sassa, A. Föhlisch, A. Lindblad, F. Schumann, S. Svensson, N. Mårtensson, The Co-ESCA station at BESSY: Auger electron–photoelectron coincidences from surfaces demonstrated for Ag MNN, J. Electron Spectrosc. Relat. Phenom. 250 (2021) 147075, http://dx.doi.org/10.1016/j.elspec.2021.147075.

[28] D. Batchelor, T. Schmidt, R. Follath, C. Jung, R. Fink, M. Knupfer, A. Schöll, T. Noll, F. Siewert, B. Büchner, E. Umbach, An energy-dispersive VUV beamline for NEXAFS and other CFS/CIS studies, Nucl. Instrum. Methods Phys. Res. A 575 (3) (2007) 470–475, http://dx.doi.org/10.1016/j.nima.2007.02.108.

[29] F. Johansson, T. Leitner, I. Bidermane, A. Born, A. Föhlisch, S. Svensson, N. Mårtensson, A. Lindblad, Auger-and photoelectron coincidences of molecular O_2 adsorbed on Ag(111), J. Electron Spectrosc. Relat. Phenom. 256 (2022) 147174.

[30] A. Preobrajenski, A. Vinogradov, N. Mårtensson, Monolayer of h-BN chemisorbed on Cu(111) and Ni(111): The role of the transition metal 3D states, Surf. Sci. 582 (1–3) (2005) 21–30.

[31] A. Born, F.O. Johansson, T. Leitner, D. Kühn, A. Lindblad, N. Mårtensson, A. Föhlisch, Separation of surface oxide from bulk Ni by selective Ni 3p photoelectron spectroscopy for chemical analysis in coincidence with Ni M-edge Auger electrons, Sci. Rep. 11 (1) (2021) 16596.

[32] A. Born, F.O. Johansson, T. Leitner, I. Bidermane, D. Kühn, N. Mårtensson, A. Föhlisch, The degree of electron itinerancy and shell closing in the core-ionized state of transition metals probed by Auger-photoelectron coincidence spectroscopy, Phys. Chem. Chem. Phys. 24 (32) (2022) 19218–19222.

[33] P.E. Blöchl, Projector augmented-wave method, Phys. Rev. B 50 (24) (1994) 17953–17979, http://dx.doi.org/10.1103/PhysRevB.50.17953.

[34] G. Kresse, J. Furthmüller, Efficient iterative schemes for ab initio total-energy calculations using a plane-wave basis set, Phys. Rev. B 54 (16) (1996) 11169–11186, http://dx.doi.org/10.1103/PhysRevB.54.11169.

[35] G. Kresse, J. Hafner, Ab initio molecular dynamics for liquid metals, Phys. Rev. B 47 (1) (1993) 558–561, http://dx.doi.org/10.1103/PhysRevB.47.558.

[36] B. Hammer, L.B. Hansen, J.K. Nsrskov, Improved adsorption energetics within density-functional theory using revised Perdew-Burke-Ernzerhof functionals, Phys. Rev. B 59 (11) (1999) 7413–7421, http://dx.doi.org/10.1103/PhysRevB.59.7413.

[37] J. Heyd, G.E. Scuseria, M. Ernzerhof, Hybrid functionals based on a screened Coulomb potential, J. Chem. Phys. 118 (18) (2003) 8207, http://dx.doi.org/10.1063/1.1564060.

[38] S. Grimme, J. Antony, S. Ehrlich, H. Krieg, A consistent and accurate ab initio parametrization of density functional dispersion correction (DFT-D) for the 94 elements H–Pu, J. Chem. Phys. 132 (15) (2010) 154104, http://dx.doi.org/10.1063/1.3382344.

[39] H.J. Monkhorst, J.D. Pack, Special points for Brillouin-zone integrations, Phys. Rev. B 13 (12) (1976) 5188–5192, http://dx.doi.org/10.1103/PhysRevB.13.5188.

[40] K. Momma, F. Izumi, VESTA 3 for three-dimensional visualization of crystal, volumetric and morphology data, J. Appl. Crystallogr. 44 (6) (2011) 1272–1276, http://dx.doi.org/10.1107/S0021889811038970.

[41] V. Wang, N. Xu, J.C. Liu, G. Tang, W.T. Geng, VASPKIT: A user-friendly interface facilitating high-throughput computing and analysis using VASP code, Comput. Phys. Comm. 267 (2021) 108033, http://dx.doi.org/10.1016/J.CPC.2021.108033.

[42] I. Fdez. Galván, M. Vacher, A. Alavi, C. Angeli, F. Aquilante, J. Autschbach, J.J. Bao, S.I. Bokarev, N.A. Bogdanov, R.K. Carlson, et al., OpenMolcas: From source code to insight, J. Chem. Theory Comput. 15 (11) (2019) 5925–5964, http://dx.doi.org/10.1021/acs.jctc.9b00532.

[43] P. Malmqvist, A. Rendell, B.O. Roos, The restricted active space self-consistent-field method, implemented with a split graph unitary group approach, J. Phys. Chem. 94 (14) (1990) 5477–5482.

[44] H. Siegbahn, L. Asplund, P. Kelfve, The Auger electron spectrum of water vapour, Chem. Phys. Lett. 35 (1975) 330.

[45] H. Ågren, U.I. Wahlgren, S. Svensson, SCF and limited CI calculations for assignment of the Auger spectrum and of the satellites in the soft X-ray spectrum of H_2O, Chem. Phys. Lett. 35 (1975) 336.

[46] E.J. McGuire, Sandia Laboratories Research Reports SC-RR-70-50, 1970.

[47] H. Ågren, On the interpretation of molecular valence Auger spectra, J. Chem. Phys. 75 (1981) 1267–1283.

[48] R. Manne, H. Ågren, Auger transition amplitudes from general many-electron wavefunctions, Chem. Phys. 93 (1985) 201–208.

[49] G. Wentzel, Z. Physik 43 (1927) 521.

[50] M. Breitschafter, E. Umbach, D. Menzel, Characterization of mixed N_2-layers on Ni(111) in the temperature range 20–100 K, Surf. Sci. 178 (1–3) (1986) 725–734.

[51] H. Ågren, On the interpretation of molecular valence Auger spectra, J. Chem. Phys. 75 (3) (1981) 1267–1283.

[52] S. Tanuma, C.J. Powell, D.R. Penn, Calculations of electron inelastic mean free paths. V. Data for 14 organic compounds over the 50–2000 eV range, Surf. Interface Anal. 21 (3) (1994) 165–176.

[53] C. Lund, S. Thurgate, A. Wedding, Intrinsic satellites in the $L_{23}VV$ Auger spectra of 3D transition metals, Phys. Rev. B 49 (16) (1994) 11352.

[54] G. Van Riessen, Z. Wei, R.S. Dhaka, C. Winkler, F.O. Schumann, J. Kirschner, Direct and core-resonant double photoemission from Cu(001), J. Phys.: Condens. Matter. 22 (9) (2010) 092201.

[55] T.-C. Chiang, G. Kaindl, T. Mandel, Layer-resolved shifts of photoemission and Auger spectra from physisorbed rare-gas multilayers, Phys. Rev. B 33 (2) (1986) 695.

[56] H. Ågren, H. Siegbahn, Semi-internal correlation in the Auger spectrum of H_2O, Chem. Phys. Lett. 69 (1980) 424–429.

[57] S.-Y. Wu, J.-J. Ho, The interaction of NO_x on Ni(111) surface investigated with quantum-chemical calculations, Phys. Chem. Chem. Phys. 12 (41) (2010) 13707–13714.

[58] G. Blyholder, CNDO model and interpretation of the photoelectron spectrum of CO chemisorbed on Ni, J. Vac. Sci. Technol. 11 (5) (1974) 865–868.

[59] J. Kiss, D. Lennon, S. Jo, J. White, Photoinduced dissociation and desorption of nitrous oxide on a platinum (111) surface, J. Phys. Chem. 95 (21) (1991) 8054–8059.

[60] D. Cortés-Arriagada, N. Villegas-Escobar, A DFT analysis of the adsorption of nitrogen oxides on Fe-doped graphene, and the electric field induced desorption, Appl. Surf. Sci. 420 (2017) 446–455.

[61] W. Griffiths, N. Correia, M. Keane, A.N. de Brito, S. Svensson, L. Karlsson, Doubly ionized states of N_2O studied by photon-induced Auger electron and double charge transfer spectroscopies, J. Phys. B: At. Mol. Opt. Phys. 24 (19) (1991) 4187.

[62] R. Murphy, W. Eberhardt, Site specific fragmentation in molecules: Auger-electron ion coincidence studies on N_2O, J. Chem. Phys. 89 (7) (1988) 4054–4057, http://dx.doi.org/10.1063/1.454839.